Hindawi
Complexity
Volume 2022, Article ID 2078372, 18 pages
https://doi.org/10.1155/2022/2078372

Research Article

Finite Difference Computation of *Au-Cu*/Magneto-Bio-Hybrid Nanofluid Flow in an Inclined Uneven Stenosis Artery

H. Thameem Basha,[1] **Karthikeyan Rajagopal**,[1] **N. Ameer Ahammad**,[2] **S. Sathish**,[3] **and Sreedhara Rao Gunakala**[4]

[1]*Centre for Nonlinear Systems, Chennai Institute of Technology, Chennai, India*
[2]*Department of Mathematics, University of Tabuk, Tabuk 71491, Saudi Arabia*
[3]*School of Mathematics and Statistics, MIT-WPU, Pune, India*
[4]*Department of Mathematics and Statistics, The University of the West Indies, St.Augustine, Kingston, Jamaica*

Correspondence should be addressed to H. Thameem Basha; thameembashah@citchennai.net

Received 21 December 2021; Accepted 8 March 2022; Published 12 April 2022

Academic Editor: Mustafa Cagri Kutlu

The present study addresses the fluid transport behaviour of the flow of gold (*Au*)-copper (*Cu*)/biomagnetic blood hybrid nanofluid in an inclined irregular stenosis artery as a consequence of varying viscosity and Lorentz force. The nonlinear flow equations are transformed into dimensionless form by using nonsimilar variables. The finite-difference technique (FTCS) is involved in computing the nonlinear transport dimensionless equations. The significant parameters like angle parameter, the Hartmann number, changing viscosity, constant heat source, the Reynolds number, and nanoparticle volume fraction on the flow field are exhibited through figures. Present results disclose that the Lorentz force strongly lessens the hybrid nanofluid velocity. Elevating the Grashof number values enhances the rate of blood flow. Growing values of the angle parameter cause to reduce the resistance impedance on the wall. Hybrid nanoparticles have a superior wall shear stress than copper nanoparticles. The heat transfer rate is amplifying at the axial direction with the growing values of nanoparticles concentration. The applied Lorentz force significantly reduces the hybrid and unitary nanofluid flow rate in the axial direction. The hybrid nanoparticles expose a supreme rate of heat transfer than the copper nanoparticles in a blood base fluid. Compared to hybrid and copper nanofluid, the blood base fluid has a lower temperature.

1. Introduction

In the physiology system, the heart is the primary organ that plays a vital role in circulating the oxygenated blood to other organs via arteries. The active and proper functioning of the heart is essential for a healthy life cycle. Improper blood transportation in the circulatory system and cardiac-related issues have been the cause of most physical illnesses and death in recent times. Based on the World Health Organization (WHO) report, 30% of deaths in 2008 were related to cardiac disease [1–3]. Most cardiac diseases are caused by cellular waste products, deposits of cholesterol, fibrin, calcium, and buildup of fatty substances in the lumen of the arteries or the formation of plaques. Such plaque formation in the arteries contributes to obstructing blood circulation flow, and this cardiac disease is perceived as stenosis. Besides, the accumulation of fatty substances on the blood vessels walls leads to heart attacks, blood clots, impeding the blood supply, myocardial infarction, and cerebral strokes. Changdar and De [4] scrutinized the impact of inclination on three different nanoparticles (silver, copper, and gold) cases in blood nanofluid flow in a multiple stenosis artery and observed that the wall exhibits low shear stress in the absence of angle parameter. Zaman et al. [5] reported the transport behaviour of silver and aluminium oxide hybrid blood nanofluid flow in a vertical stenotic artery and showed that the unity nanofluid has a higher temperature than the hybrid nanofluid. Tripathi et al. [6] utilized the explicit

forward time step approach to scrutinize the flow of gold (Ag)-silver (Au)/blood hybrid nanofluid in irregular stenosis with the variable viscosity and noted that the variable viscosity parameter promotes the hybrid nanofluid axial velocity. Das et al. [7] explained the impacts of Hall current and inclination on hybrid blood nanofluid flow in a mild stenosis artery and reported that the growing values of the Grashof number elevate the blood velocity. Some studies about the blood fluid flow can be found in references [8–17].

The physiological fluids that are affected by the external magnetic field and magnetization are dubbed biomagnetic fluids. In recent times, researchers give much attention to the examination of biomagnetic fluid because it has significant applications in biomedical and bioengineering, including targeted drug delivery, cell separation, magnetic wound treatment, reduction of bleeding during surgeries, medical devices (magnetic tracers and blood pumps), and magnetic hyperthermia. It is noticed that the blood is one of the relevant examples of a biomagnetic fluid because it have the cell membrane, haemoglobin compound interface, and intercellular protein. Besides, the unadulterated blood is experienced less impact with the magnetic field. Therefore, in such cases, notable magnetic fields strength is essential to influence its flow. It is observed that artificially suspending nanoparticles with magnetic behaviour can greatly promote the magnetization of the blood. Further, blood containing such magnetic nanoparticles refuses the diamagnetic material or discarding paramagnetic and leads to behaving as a ferromagnetic fluid; as a result, fluid velocity rises gradually. Misra and Shit [18] addressed the influence of magnetic dipole on the flow of viscoelastic biomagnetic fluid past an extending surface and observed that the ferromagnetic interaction parameter diminishes the biomagnetic axial velocity. Murtaza et al. [19] performed a numerical study with the aim to express fluid transport behaviour of maxwell biomagnetic fluid flow over an extending surface and pointed out the rate of heat transfer is reduced with the rising values of magnetic field. Maiti et al. [20] employed the Caputo-Fabrizio (CF) derivative model to examine the biomagnetic blood fluid flow in a porous vessel and found that the thermal radiation and the Schmidt number decline the blood concentration. The flow of biomagnetic fluid through a normal duct in the presence of magnetic dipole and Lorentz force was scrutinized by Mousavi et al. [21] and noticed that the Lorentz force near the constricted zone lessens the wall shear stress. Some notable studies on blood flow with the impact of the magnetic field are exposed through Refs. [22–29].

Numerous researchers and engineers have paid significant attention to nanotechnology because it is used in several practical situations, for instance, biochemical engineering and medical industries. Several nanoparticles like silver, copper, gold, and ferrite particles are utilized in proteins, delivery of drugs, nucleic acids, vaccines, and genes [30–33]. Because these nanoparticles exhibit high biocompatibility, magnetic, chemical, unique mechanical, and thermal effects. It is observed that gold (atomic number = 79) nanoparticles have much popularity in biomedical applications for RNA quantification (via optical biosensors) and treating malignant tumours owing to unique quenching efficiencies, targeting ligands, significant surface modifiability, and imaging probes when comparing with other nanoparticles [34–38]. Besides, the gold nanoparticles exhibit a nontoxic behaviour in biological media. Gold nanoparticles have a unique optical behavior, which is more relevant for several therapeutic applications (photothermal and radiotherapy for eradicating cancer cells) and diagnostic approaches (cell imaging, computed tomography, and optical imaging). It is important to mention that the gold nanoparticles can be remarkably functionalized with DNA, proteins, antibodies, polyelectrolyte, and ligands. Koriko et al. [39] examined the heat transfer behaviour of gold-blood Carreau nanofluid flow with the influence of partial slip and that the elevating gold nanoparticle concentration tends to diminish the rate of heat transfer. Kumar and Srinivas [40] employed the Maxwell Garnett and Brinkman models (thermophysical property model) to analyze the flow of gold blood nanofluid in a channel and found that the gold nanoparticles have a less temperature in the blood than the aluminium oxide. Khan et al. [41] conducted a numerical study to determine the impact of nonlinear radiation on Casson gold–blood nanofluid flow over an extending spinning disk and noticed that the blood temperature rises by elevating nanoparticle volume fraction. Bhatti [42] explored the Jeffrey-gold intrauterine nanofluid flow through an asymmetric channel by means of linear thermal radiation and showed that thermal radiation maximizes Jeffrey blood temperature. Most science and engineering problems are usually in the form of nonlinear boundary value problems (BVPs). The solution of such nonlinear problems plays a significant role in understanding science and engineering systems. It is noticed that most of the nonlinear BVPs are partial differential equations (PDEs). Numerous numerical and analytical approaches are available in the literature to solve such PDEs. In that, the explicit finite-difference FTCS method is one of the notable approaches, and it is described in Hoffmann's book [43]. It is essential to mention that many researchers extensively used FTCS in fluid mechanical and biomechanical problems [44, 45]. Further, it is revealed that this scheme is stable, rapidly convergent, and easy to program.

The motivation of this current analysis is that for the applications in targeted nano-drug delivery systems. Besides, this numerical simulation's primary purpose is to effectively carry out the decision-making process during arterial disease treatment. In recent times, targeting the nano-drugs at the stenosis region is the trending and influential approach compared to the conventional treatment method. The nano-drug delivery improves the stenosis throat's clotting formation; further, this computational simulation can also predict the effects of post-treatment processes. It is witnessed from the above literature that several studies explore the blood flow in different types of stenosis arteries with numerous physical aspects. However, no study has focused on the gold and copper/blood nanofluid flow in an uneven inclined stenosis artery in the presence of a magnetic field, viscous dissipation, and heat generation. Further, the gold and copper [46, 47] nanoparticles have predominant

applications in drug targeting, wound treatment, cancer diagnosis, cardiovascular treatment, and chemotherapy. With these enthused, the current framework focuses on biomagnetic gold-copper blood hybrid nanofluid flow in an irregular inclined stenosis artery utilizing varying viscosity and Lorentz force. By means of nonsimilar variables, the dimensional flow equations are reduced in dimensionless form. The finite-difference approach is executed to compute the reduced flow equations. The physical parameters that arise from the regime equations are projected through graphs.

2. Mathematical Formulation

This model considers time-dependent two-dimensional biomagnetic gold-copper hybrid nanofluid flow in an inclined irregular stenosis artery, and the schematic model is exhibited in Figure 1. The nanoparticle volume fraction model is utilized to scrutinize the biomagnetic blood flow. It is noted that the gold and copper nanoparticles are suspended in the biomagnetic blood fluid, and the thermophysical properties of the base fluid (blood) and nanomaterial (gold and copper) are provided in Table 1. The strength of Lorentz force is executed in the transverse to the blood flow direction. For this modelling, the two-dimensional cylindrical coordinate (r, θ, z) system is employed, and r and z are represented as the artery radial and axial coordinates (Tripathi et al. [6]).

$$R(z) = \begin{cases} R_0 - 2\delta\left[\cos\left(\left(\frac{z-d}{2} - \frac{l_0}{4}\right)2\pi\right) - \frac{7}{100}\cos\left(\left(z - d - \frac{l_0}{2}\right)32\pi\right)\right], & d < z < d + l_0 \\ R_0, \quad \text{otherwise} \end{cases}, \tag{1}$$

where δ is the stenosis depth, d is the stenosis distance from origin, z is the axial co-ordinate, and l_0 is the stenosis length.

In this model, the blood nanofluid flowing is unsteady and bidirectionally; the velocity and temperature can be expressed as

$$\begin{aligned} &\text{Velocity: } V = [\overline{u}(r,z,t), 0, \overline{w}(r,z,t)], \\ &\text{Temperature: } T = T(r,z,t). \end{aligned}, \tag{2}$$

where $\overline{u}$ and $\overline{w}$ have denoted the of components radial and axial velocities. With these frameworks, the governing flow equations are written as follows (Zaman et al. [5], Tripathi et al. [6, 45], Das et al. [7], and Rathore and Srikanth [16]):

$$\frac{\partial \overline{u}}{\partial \overline{r}} + \frac{\overline{u}}{\overline{r}} + \frac{\partial \overline{w}}{\partial \overline{z}} = 0. \tag{3}$$

$$\begin{aligned} (\rho_{\text{hnf}})\left(\frac{\partial \overline{u}}{\partial \overline{t}} + \overline{u}\frac{\partial \overline{u}}{\partial \overline{r}} + \overline{w}\frac{\partial \overline{u}}{\partial \overline{z}}\right) = &-\frac{\partial \overline{p}}{\partial \overline{r}} + \frac{1}{\overline{r}}\left[\frac{\partial}{\partial \overline{r}}\left(\mu_{\text{hnf}}(T)\frac{\partial \overline{u}}{\partial \overline{r}}\right) - 2\mu_{\text{hnf}}(T)\frac{\overline{u}}{\overline{r}}\right] \\ &+ \frac{\partial}{\partial \overline{z}}\left(\mu_{\text{hnf}}(T)\left(\frac{\partial \overline{u}}{\partial \overline{z}} + \frac{\partial \overline{w}}{\partial \overline{r}}\right)\right) - g(\gamma\rho)_{\text{hnf}}(T - T_1)\cos(\alpha). \end{aligned} \tag{4}$$

$$\begin{aligned} (\rho_{\text{hnf}})\left(\frac{\partial \overline{w}}{\partial \overline{t}} + \overline{u}\frac{\partial \overline{w}}{\partial \overline{r}} + \overline{w}\frac{\partial \overline{w}}{\partial \overline{z}}\right) = &-\frac{\partial \overline{p}}{\partial \overline{z}} + \frac{1}{\overline{r}}\frac{\partial}{\partial \overline{r}}\left(r\mu_{\text{hnf}}(T)\left(\frac{\partial \overline{u}}{\partial \overline{z}} + \frac{\partial \overline{w}}{\partial \overline{r}}\right)\right) \\ &+ \frac{\partial}{\partial \overline{z}}\left(2\mu_{\text{hnf}}(T)\frac{\partial \overline{w}}{\partial \overline{z}}\right) + g(\gamma\rho)_{\text{hnf}}(T - T_1)\sin(\alpha) - \sigma_{\text{hnf}}B_0^2 w. \end{aligned} \tag{5}$$

$$\left(\rho C_p\right)_{\text{hnf}}\left(\frac{\partial T}{\partial \overline{t}} + \overline{u}\frac{\partial T}{\partial \overline{r}} + \overline{w}\frac{\partial T}{\partial \overline{z}}\right) = k_{\text{hnf}}\left(\frac{\partial^2 T}{\partial \overline{r}^2} + \frac{1}{\overline{r}}\frac{\partial T}{\partial \overline{r}} + \frac{\partial^2 T}{\partial \overline{z}^2}\right) + Q_0. \tag{6}$$

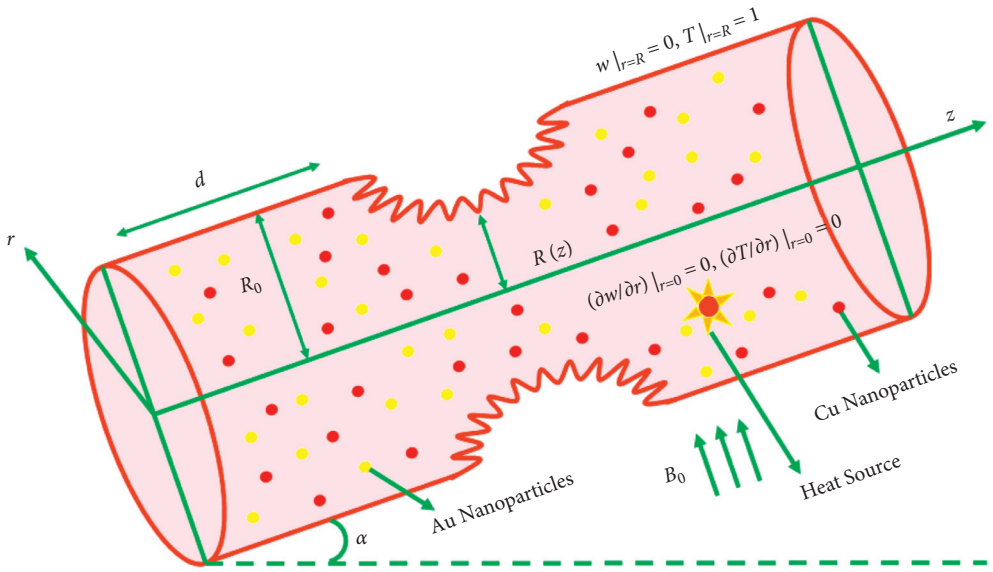

Figure 1: Physical configuration of the problem.

Table 1: Values of the various physical parameters (blood, gold and copper) (Das et al. [7], Koriko [39], and Kumar and Srinivas [40]).

Physical properties	Blood	Gold (Au)	Copper (Cu)
ρ (kg/m^3)	1063	19320	8933
C_p (J/kgK)	3594	129	385
$\gamma \times 10^{-5}$ (K^{-1})	0.18	1.4	1.67
k (W/mK)	0.492	314	401
σ (S/m)	6.67×10^{-1}	4.10×10^{7}	59.6×10^{6}

In the foregoing equation, α is the angle parameter, Q_0 is the constant heat source parameter, B_0 is the uniform magnetic field, ρ_{hnf} is the density, $\overline{t}$ is the time, $\overline{p}$ is the pressure, $\overline{r}$ is the radial coordinate, k_{hnf} is the thermal conductive, μ_{hnf} is the dynamic viscosity, T is the temperature, γ_{hnf} is the thermal expansion, g is the gravitational acceleration, σ_{hnf} is the electrical conductivity, $(C_p)_{\mathrm{hnf}}$ is the specific heat capacity, and subscript hnf is the hybrid nanofluid.

The relevant limiting conditions are expressed as follows:

$$\left.\begin{aligned} w(R,t) = 0, \frac{\partial w(0,t)}{\partial r} = 0, w(r,0) = 0, \\ T(R,t) = 1, \frac{\partial T(0,t)}{\partial r} = 0, T(r,0) = 0. \end{aligned}\right\}. \tag{7}$$

The governing nonlinear flow equations are transformed by suitable nonsimilar variables, which are shown as follows (Zaman et al. [5] and Tripathi et al. [6, 45]):

$$\begin{aligned} r &= \frac{\overline{r}}{R_0}, \\ z &= \frac{\overline{z}}{l_0}, \\ \overline{p} &= \frac{R_0^2 P}{U_0 l_0 \mu_f}, \\ u &= \frac{l_0 \overline{u}}{\delta^* U_0}, \\ \theta &= \frac{T - T_1}{T_w - T_1}, \\ w &= \frac{\overline{w}}{U_0}, \\ R &= \frac{\overline{R}}{R_0}, \\ t &= \frac{U_0 \overline{t}}{R_0}, \\ d &= \frac{\overline{d}}{l_0}. \end{aligned} \tag{8}$$

Here, U_0 is the reference velocity, $G_r = g\rho_f R_0^2 \gamma_f (T_w - T_1)/U_0\mu_f$ is the Grashof number, T_w is the wall temperature, $M_a = \sqrt{\sigma_f/\mu_f} B_0 R_0$ is the Hartmann number, $\varepsilon = R_0/l_0$ is the vessel aspect ratio, $\Pr = (C_p)_f \mu_f / k_f$ is the Prandtl number, $\delta = \delta^*/R_0$ is the stenosis height parameter, and $R_e = U_0\rho_f R_0/\mu_f$ is the Reynolds number.

By employing the above variables in equations (3)–(6), the transformed equations are as follows:

$$
\begin{aligned}
&\delta\left(\frac{\partial u}{\partial r} + \frac{u}{r}\right) + \frac{\partial w}{\partial z} = 0,\\
&R_e\left(\frac{\rho_{\mathrm{hnf}}}{\rho_f}\right)\delta\varepsilon^2\left(\frac{\partial u}{\partial t} + (\delta\varepsilon)u\frac{\partial u}{\partial r} + \varepsilon w\frac{\partial u}{\partial z}\right) = -\frac{\partial p}{\partial r} + \left(\frac{\delta R_0}{l_0^2\mu_0}\right)\frac{1}{r}\frac{\partial}{\partial r}\left(\mu_{\mathrm{hnf}}(\theta)\frac{\partial u}{\partial r}\right)\\
&+\left(\frac{\varepsilon^2 R_0}{\mu_0}\right)\frac{\partial}{\partial z}\left(\mu_{\mathrm{hnf}}(\theta)\left(\frac{\delta\varepsilon}{l_0}\frac{\partial u}{\partial z} + \frac{1}{R_0}\frac{\partial w}{\partial r}\right)\right)\\
&-2\left(\frac{\delta\varepsilon^2}{\mu_0}\right)\mu_{\mathrm{hnf}}(\theta)\left(\frac{u}{r^2}\right) - \left(\frac{(\rho\gamma)_{\mathrm{hnf}}}{(\rho\gamma)_f}\right)\varepsilon\cos(\alpha)G_r\theta,\\
&R_e\left(\frac{\rho_{\mathrm{hnf}}}{\rho_f}\right)\left(\frac{\partial w}{\partial t} + (\delta\varepsilon)u\frac{\partial w}{\partial r} + \varepsilon w\frac{\partial w}{\partial z}\right) = -\frac{\partial p}{\partial z} + \frac{1}{r}\frac{\partial}{\partial r}\left(\frac{r\mu_{\mathrm{hnf}}(\theta)}{\mu_0}\left\{\delta\varepsilon^2\frac{\partial u}{\partial z} + \frac{\partial w}{\partial r}\right\}\right)\\
&+\varepsilon^2\frac{\partial}{\partial z}\left(\frac{2\mu_{\mathrm{hnf}}(\theta)}{\mu_0}\frac{\partial w}{\partial z}\right) + \left(\frac{(\rho\gamma)_{\mathrm{hnf}}}{(\rho\gamma)_f}\right)G_r\theta\sin(\alpha) - \frac{\sigma_{\mathrm{hnf}}}{\sigma_f}M_a^2 w,\\
&R_e\Pr\left(\frac{k_f}{k_{\mathrm{hnf}}}\right)\left(\frac{\left(\rho C_p\right)_{\mathrm{hnf}}}{\left(\rho C_p\right)_f}\right)\left(\frac{\partial\theta}{\partial t} + (\delta\varepsilon)u\frac{\partial\theta}{\partial r} + \varepsilon w\frac{\partial\theta}{\partial z}\right)\\
&= \left(\frac{\partial^2\theta}{\partial r^2} + \frac{1}{r}\frac{\partial\theta}{\partial r} + \varepsilon^2\frac{\partial^2\theta}{\partial z^2}\right) + \left(\frac{k_f}{k_{\mathrm{hnf}}}\right)\beta.
\end{aligned}
\tag{9}
$$

Usually, in a biological system, the viscosity of blood is not constant in all cases since it varies due to several factors such as hematocrit ratio, vessel width, temperature, and axial or radial coordinates. Such a viscosity variation causes several reality cases, including decreasing blood thickness, rising of blood circulation, lowering coagulation factors, and maximizing blood flow. To capture these behaviours, in this model, the blood nanofluid viscosity is considered dependent on fluid temperature, which is given as (Zaman et al. [5])

$$
\mu_f(\theta) = \mu_0 e^{-\eta_0\theta}, \quad \text{where } e^{-\eta_0\theta} = 1 - \eta_0\theta, \quad \eta_0 \ll 1, \tag{10}
$$

where η_0 is the viscosity constant.

The density, thermal conductivity, electrical conductivity, thermal expansion, dynamic viscosity, and specific heat capacity of the nanofluid and hybrid nanofluid are (Tripathi et al. [6] and Das et al. [7])

$$
\left.
\begin{aligned}
&\rho_{\mathrm{nf}} = \phi\rho_s + (1-\phi)\rho_f, \sigma_{\mathrm{nf}} = \sigma_f\left(\frac{3\left(\sigma_s/\sigma_f - 1\right)\phi}{\left(\sigma_s/\sigma_f + 2\right) - \phi\left(\sigma_s/\sigma_f - 1\right)} + 1\right),\\
&\left(\rho C_p\right)_{\mathrm{nf}} = \phi\left(\rho C_p\right)_s + (1-\phi)\left(\rho C_p\right)_f, \mu_{\mathrm{nf}} = \frac{\mu_f}{(1-\phi)^{2.5}},\\
&k_{\mathrm{nf}} = k_f\left(\frac{k_s + 2k_f - 2\phi\left(k_f - k_s\right)}{k_s + 2k_f + \phi\left(k_f - k_s\right)}\right), (\rho\gamma)_{\mathrm{nf}} = \phi(\rho\gamma)_s + (1-\phi)(\rho\gamma)_f.
\end{aligned}
\right\},
$$

$$\left.\begin{aligned}
&\rho_{\mathrm{hnf}} = \left(\phi_1\rho_{s_1} + (1-\phi_1)\rho_f\right)(1-\phi_2) + \phi_2\rho_{s_2}, \mu_{\mathrm{hnf}} = \frac{\mu_f(\theta)}{(1-\phi_1)^{2.5}(1-\phi_2)^{2.5}},\\
&\frac{\sigma_{\mathrm{hnf}}}{\sigma_{\mathrm{bf}}} = \frac{\sigma_{s_2} + 2\sigma_{\mathrm{bf}} - 2\phi_2\left(\sigma_{\mathrm{bf}} - \sigma_{s_2}\right)}{\sigma_{s_2} + 2\sigma_{\mathrm{bf}} + \phi_2\left(\sigma_{\mathrm{bf}} - \sigma_{s_2}\right)}, \frac{k_{\mathrm{hnf}}}{k_{\mathrm{bf}}} = \frac{k_{s_2} + 2k_{\mathrm{bf}} - 2\phi_2\left(k_{\mathrm{bf}} - k_{s_2}\right)}{k_{s_2} + 2k_{\mathrm{bf}} + \phi_2\left(k_{\mathrm{bf}} - k_{s_2}\right)},\\
&\left(\rho C_p\right)_{\mathrm{hnf}} = \left(\phi_1\left(\rho C_p\right)_{s_1} + (1-\phi_1)\left(\rho C_p\right)_f\right)(1-\phi_2) + \phi_2\left(\rho C_p\right)_{s_2},\\
&(\rho\gamma)_{\mathrm{hnf}} = \left(\phi_1(\rho\gamma)_{s_1} + (1-\phi_1)(\rho\gamma)_f\right)(1-\phi_2) + \phi_2(\rho\gamma)_{s_2},\\
&\text{where } \frac{\sigma_{\mathrm{bf}}}{\sigma_f} = \frac{\sigma_{s_1} + 2\sigma_f - 2\phi_1\left(\sigma_f - \sigma_{s_1}\right)}{\sigma_{s_1} + 2\sigma_f + \phi_1\left(\sigma_f - \sigma_{s_1}\right)}, \frac{k_{\mathrm{bf}}}{k_f} = \frac{k_{s_1} + 2k_f - 2\phi_1\left(k_f - k_{s_1}\right)}{k_{s_1} + 2k_f + \phi_1\left(k_f - k_{s_1}\right)}.
\end{aligned}\right\}, \tag{11}$$

where μ_f, σ_f, $(C_p)_f$, ρ_f, γ_f, and k_f are the viscosity, electrical conductivity, specific heat capacity, density, thermal expansion, and thermal conductivity of the base fluid, (ϕ_1, ϕ_2) is the nanoparticle volume fraction, subscript s_1, bf, and s_2 are the first solid particle, base fluid, and second solid particle.

It is observed that compared with the artery radius, the stenosis maximum height is small, and the further length of the stenotic region and artery radius is of comparable magnitude. Therefore, the dimensionless flow equations are minimized with the following hypothesis $\delta \ll 1$ and $\varepsilon = \mathrm{O}(1)$. By employing these hypotheses, the reduced equations are

$$\frac{\partial w}{\partial z} = 0,$$

$$\frac{\partial p}{\partial r} = 0,$$

$$R_e\left(\frac{\rho_{\mathrm{hnf}}}{\rho_f}\right)\left(\frac{\partial w}{\partial t}\right) = -\left(\frac{\partial p}{\partial z}\right) + \frac{1}{r}\frac{\partial}{\partial r}\left(\frac{r\mu_{\mathrm{hnf}}(\theta)}{\mu_0}\left(\frac{\partial w}{\partial r}\right)\right)$$

$$+\left(\frac{(\rho\gamma)_{\mathrm{hnf}}}{(\rho\gamma)_f}\right)G_r\theta\,\sin(\alpha) - \frac{\sigma_{\mathrm{hnf}}}{\sigma_f}M_a^2 w, \tag{12}$$

$$R_e\left(\frac{\left(\rho C_p\right)_{\mathrm{hnf}}}{\left(\rho C_p\right)_f}\right)\left(\frac{k_f}{k_{\mathrm{hnf}}}\right)\mathrm{Pr}\left(\frac{\partial\theta}{\partial t}\right) = \left(\frac{\partial^2\theta}{\partial r^2} + \frac{1}{r}\frac{\partial\theta}{\partial r}\right) + \left(\frac{k_f}{k_{\mathrm{hnf}}}\right)\beta,$$

$$R(z) = \left\{\begin{array}{ll} 1 - 2\delta^*\left[\cos\left(\left(\frac{(z-d)}{2} - \frac{1}{4}\right)2\pi\right) - \cos\left(\left(z - d - \frac{1}{2}\right)32\pi\right)\left(\frac{7}{100}\right)\right], & d < \overline{z} < d+1 \\ 1, & \text{otherwise} \end{array}\right\}.$$

According to Burton [48], the pulsatile pressure gradient is denoted as

$$-\frac{\partial p}{\partial z} = A_0 + A_1 t\,\cos\left(2\pi\omega_p\right), \quad t > 0, \tag{13}$$

where A_0 represents the mean pressure gradient and A_1 represents the amplitude of the pulsatile component that controls systolic and diastolic pressures.

By employing (8) in (13), the simplified equation is

$$-\frac{\partial p}{\partial z} = B_1\left(1 + e\,\cos\left(c_1 t\right)\right), \tag{14}$$

where $e = A_1/A_0, B_1 = A_0 a^2/\mu_0 U_0$ and $c_1 = 2\pi\,\mathrm{aw}_p/U_0$.

Incorporating the (14) in the blood hybrid nanofluid axial velocity, one can get:

$$R_e\left(\frac{\rho_{\mathrm{hnf}}}{\rho_f}\right)\left(\frac{\partial w}{\partial t}\right) = B_1\left(1 + e\,\cos\left(c_1 t\right)\right) + \frac{1}{r}\frac{\partial}{\partial r}\left(\frac{r\mu_{\mathrm{hnf}}(\theta)}{\mu_0}\left(\frac{\partial w}{\partial r}\right)\right) + \left(\frac{(\rho\gamma)_{\mathrm{hnf}}}{(\rho\gamma)_f}\right)G_r\theta\,\sin(\alpha) - \frac{\sigma_{\mathrm{hnf}}}{\sigma_f}M_a^2 w. \tag{15}$$

The set of equations are transformed in the radial coordinate $(x = r/R(z))$ form since the governing flow equations are incorporated with limiting conditions:

$$\begin{aligned} &R_e\left(\frac{\rho_{\mathrm{hnf}}}{\rho_f}\right)\left(\frac{\partial w}{\partial t}\right) = B_1\left(1 + e\,\cos\left(c_1 t\right)\right) + \left(\frac{\mu_{\mathrm{hnf}}(\theta)}{\mu_0}\right)\\ &\frac{1}{R^2}\left(\frac{\partial^2 w}{\partial x^2} + \frac{1}{x}\frac{\partial w}{\partial x}\right) + \left(\frac{(\rho\gamma)_{\mathrm{hnf}}}{(\rho\gamma)_f}\right)\\ &G_r\theta\,\sin(\alpha) - \frac{\sigma_{\mathrm{hnf}}}{\sigma_f}M_a^2 w,\\ &\left(\frac{\left(\rho C_p\right)_{\mathrm{hnf}}}{\left(\rho C_p\right)_f}\right)\left(\frac{k_f}{k_{\mathrm{hnf}}}\right)R_e\mathrm{Pr}\left(\frac{\partial\theta}{\partial t}\right)\\ &= \frac{1}{R^2}\left(\frac{\partial^2\theta}{\partial x^2} + \frac{1}{x}\frac{\partial\theta}{\partial x}\right) + \left(\frac{k_f}{k_{\mathrm{hnf}}}\right)\beta. \end{aligned} \tag{16}$$

The radial coordinate form of boundary conditions are

$$\begin{aligned} &x = 0\colon \frac{\partial w(0,t)}{\partial x} = 0, \frac{\partial\theta(0,t)}{\partial x} = 0,\\ &x = 1\colon w(1,t) = 0, \theta(1,t) = 1,\\ &t = 0\colon w(x,0) = 0, \theta(x,0) = 0. \end{aligned} \tag{17}$$

Wall shear stress (τ_s), the Nusselt number (Nu^*), volumetric flow rate (Q_F), and resistance impedance (λ) of the present model are written as

$$\left.\begin{aligned} &\tau_s = -\frac{1}{R(z)}\left(\frac{\partial w}{\partial x}\right)_{x=1},\\ &\mathrm{Nu}^* = -\frac{1}{R(z)}\left(\frac{\partial\theta}{\partial x}\right)_{x=1},\\ &Q_F = (R(z))^2 2\pi\left(\int_0^1 \mathrm{wx}\,\mathrm{d}x\right),\\ &\lambda = L\left[\frac{(\partial p/\partial z)}{Q_F}\right] = L\left[\frac{B_1\left(1 + e\,\cos(2\pi t)\right)}{(R(z))^2 2\pi\left(\int_0^1 \mathrm{wx}\,\mathrm{d}x\right)}\right]. \end{aligned}\right\} \tag{18}$$

3. Numerical Method

The FTCS (forward time central space) finite-difference technique is employed to solve the present mathematical model's nonlinear coupled dimensionless flow equations subject to the appropriate initial and boundary condition. A rectangular region of the flow field is chosen in the explicit approach. The region is divided into a grid of lines parallel to axes, and it is displayed in Figure 2. The spatial domain is first discretized in this approach and after that the velocity and temperature values are obtained from each node x_j. Besides, instant step t^i is found over the time. The first derivative is discretized by forward differencing and the second derivative for central differencing. The $N + 1$ steps are used to discretize the spatial variable with the $\Delta x/N + 1$ step size. t^i expresses the time change, and $t^i = \Delta t\,(i - 1)$ finds its value. It is noticed that the Δt is a small difference in time. The blood velocity and the temperature are calculated in a different time step.

$$\left.\begin{aligned} &\frac{\partial w}{\partial t} \cong \frac{w_j^{i+1} - w_j^i}{\Delta t}; \frac{\partial\theta}{\partial t} \cong \frac{\theta_j^{i+1} - \theta_j^i}{\Delta t}\\ &\frac{\partial w}{\partial x} \cong \frac{w_{j+1}^i - w_{j-1}^i}{2\Delta x}; \frac{\partial\theta}{\partial x} \cong \frac{\theta_{j+1}^i - \theta_{j-1}^i}{2\Delta x}\\ &\frac{\partial^2 w}{\partial x^2} \cong \frac{w_{j+1}^i - 2w_j^i + w_{j-1}^i}{2\Delta x}; \frac{\partial^2\theta}{\partial x^2} \cong \frac{\theta_{j+1}^i - 2\theta_j^i + \theta_{j-1}^i}{2\Delta x} \end{aligned}\right\}. \tag{19}$$

By employing the above expression, the discretized form of equations is written as follows:

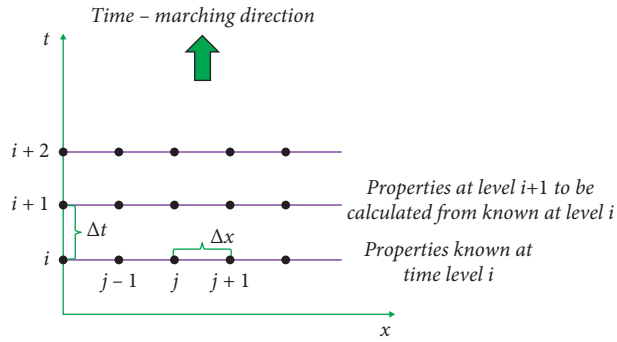

Figure 2: Finite difference space grid.

$$w_j^{i+1} = w_j^i + \frac{\Delta t}{R_e\left(1-\phi_2\left[(1-\phi_1)+\phi_1\left(\rho_{s_1}/\rho_f\right)\right]+\phi_2\rho_{s_2}/\rho_f\right)}\left[\begin{array}{c} B_1\left(1+e\,\cos\left(c_1 t^i\right)\right)+\dfrac{\left(1-\eta_0\theta_j^i\right)}{\left(1-\phi_1\right)^{2.5}\left(1-\phi_2\right)^{2.5}} \\ \left(\dfrac{1}{R^2}\right)\left(\dfrac{\partial^2 w}{\partial x^2}+\dfrac{1}{x}\dfrac{\partial w}{\partial x}\right) \\ +\left(1-\phi_2\left[(1-\phi_1)+\phi_1\left(\dfrac{(\rho\gamma)_{s_1}}{(\rho\gamma)_f}\right)\right]+\phi_2\dfrac{(\rho\gamma)_{s_2}}{(\rho\gamma)_f}\right) \\ G_r\theta_j^i\sin(\alpha)-\dfrac{\sigma_{\mathrm{hnf}}}{\sigma_f}M_a^2 w_j^i \end{array}\right], \tag{20}$$

$$\theta_j^{i+1} = \theta_j^i + \frac{\left(k_{\mathrm{hnf}}/k_f\right)\Delta t}{R_e\mathrm{Pr}\left(1-\phi_2\left[(1-\phi_1)+\phi_1\left(\left(\rho C_p\right)_{s_1}/\left(\rho C_p\right)_f\right)\right]+\phi_2\left(\rho C_p\right)_{s_2}/\left(\rho C_p\right)_f\right)}$$
$$\left\{\frac{1}{R^2}\left(\frac{\partial^2\theta}{\partial x^2}+\frac{1}{x}\frac{\partial\theta}{\partial x}\right)+\left(\frac{k_f}{k_{\mathrm{hnf}}}\right)\beta\right\}.$$

With the boundary conditions are

$$\left.\begin{array}{ll} w_j^1=\theta_j^1=0, & \text{at } t=0, \\ w_{j+1}^i=w_j^i,\ \theta_{j+1}^i=\theta_j^i, & \text{at } x=0, \\ w_{N+1}^i=0,\ \theta_{N+1}^i=1, & \text{at } x=1. \end{array}\right\}. \tag{21}$$

The stability of this scheme completely depends on time increment (Δt) and step size (Δx); thus, $\Delta t = 0.0001$ and $\Delta x = 0.025$ are fixed to tackle the stability condition. Several studies [5, 6, 43, 45, 46] proved that these values are suitable for stability and convergence of the FTCS approach. Further, Hoffmann's book [43] exposed that the above-used time and spatial values confirm this scheme's stability and convergence. Figure 3 (*a*) and Figure 3 (*b*) shows the local error and sum of time and space error on the dimensionless radius, respectively. From these figures, it is observed that the velocity and temperature of blood maintain 10^{-10} error at each spatial node. As similar, the sum of time and space error is 10^{-6}. This is evidence that the current numerical approach provides efficient results. The FTCS approach has been employed in numerous previous simulations, including heat transfer enhancement for solar energy absorber in a permeable annular [49], the blood flow of viscoelastic fluid in tapered overlapping even stenosed artery [50], and the exploration of nano-Bingham-Papanastasiou fluid in a diseased curved artery [51]. The studies manifest above have extensively validated that the FTCS approach is efficient for blood flow computation in complex geometries.

4. Results and Discussion

This section affords the physical aspects of emerging parameters like variable viscosity ($\eta_0 = 0, 0.1, 0.3, 0.5$), constant heat source ($\beta = 0, 0.3, 0.6, 0.9$), angle parameter ($\alpha = 0, \pi/6, \pi/4, \pi/2$), the Hartmann number

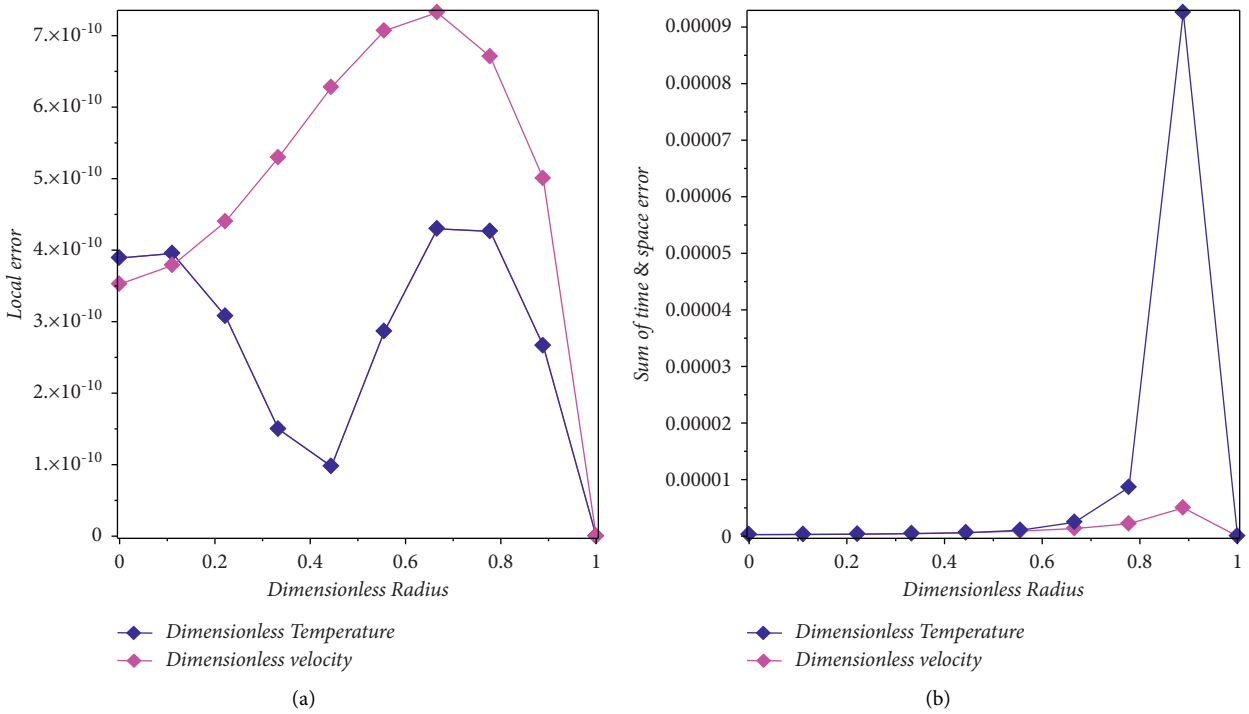

Figure 3: (a) Local error on w and θ. (b) Sum of time and space error on w and θ.

($M_a = 1, 2, 3, 4$), the Grashof number ($G_r = 0, 0.1, 0.3, 0.5$), the Reynolds number ($R_e = 2, 3, 4, 5$), and nanoparticle volume fraction ($\phi_1 + \phi_2 = 0.01, 0.02, 0.03, 0.05$) on the biomagnetic blood hybrid nanofluid velocity (w), temperature (θ), resistance impedance (λ), wall shear stress (τ_s), the Nusselt number (Nu^*), and volumetric flow rate (Q_F). The parametric values [4, 5, 6, 46] such as $B_1 = 1.41$, $d = 0.5$, $\delta^* = 0.1$, $e = 0.5$, $\mathrm{Pr} = 14$, $c_1 = 1$, $\beta = 0.1$, $G_r = 0.5$, $R_e = 2$, $M_a = 0.5$, $\alpha = \pi/2$, $\eta_0 = 0.2$, $\phi_1 = 0.025$, and $\phi_2 = 0.025$ are considered for computation. In this model, the significance of gold-copper hybrid nanofluid and copper nanofluid characteristics is analyzed via graphs. The system of equations is reduced with the help of nonsimilar variables, and FTCS obtains the solution. For obtaining scheme validation, the present result is compared with earlier results in Table 2. It is witnessed that the present results are in valid agreement. It is essential to note that the hybrid nanofluid turns into a mono nanofluid in the absence of gold nanoparticles ($\phi_1 = 0$). To show the variation in figures, the solid line is used for the hybrid nanofluid case, and the dashed line is used for the nanofluid case. The behaviour of the base fluid, nanofluid, and hybrid nanofluid on temperature is compared in Table 3. This table shows that the blood base fluid generates a lower temperature than the nanofluid and hybrid nanofluid cases.

Variation of the Reynolds number (R_e) on biomagnetic blood hybrid nanofluid axial velocity and temperature is visualised for hybrid nanofluid and Cu nanofluid cases in Figures 4 and 5, respectively. In this study, due to the laminar flow case, meagre Reynolds numbers are assumed, so the viscosity is dominant in the regime. It is clear from these figures that the biomagnetic blood axial velocity significantly

Table 2: Validation of biomagnetic blood axial velocity with Zaman et al. [5] and Tripathi et al. [6].

R	Zaman et al. [5]	Tripathi et al. [6]	Present result
0	0.5859	0.5881	0.58900
0.1	0.5829	0.5845	0.58289
0.2	0.5725	0.5725	0.57170
0.3	0.5540	0.5518	0.55339
0.4	0.5261	0.5215	0.52593
0.5	0.4864	0.4802	0.48727
0.6	0.4323	0.4257	0.43843
0.7	0.3605	0.3549	0.37083
0.8	0.2671	0.2637	0.27891
0.9	0.1483	0.1473	0.15715
1.0	0	0	0

Table 3: Comparison of base fluid, nanofluid, and hybrid nanofluid on temperature.

R	Temperature		
	Blood basefluid	*Cu*/blood nanofluid	*Au-Cu*/blood hybrid nanofluid
0	0.060607	0.092054	0.093989
0.1	0.067032	0.099859	0.101855
0.2	0.087374	0.124016	0.126176
0.3	0.124622	0.166525	0.168902
0.4	0.182908	0.229936	0.232505
0.5	0.266231	0.316289	0.318937
0.6	0.376797	0.425898	0.428428
0.7	0.513356	0.556286	0.558456
0.8	0.670114	0.701653	0.703227
0.9	0.836782	0.853146	0.853959
1.0	1	1	1

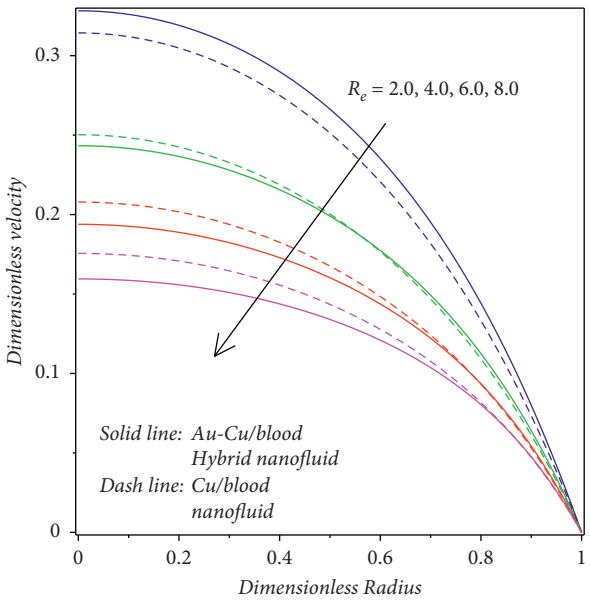

Figure 4: Behaviour of R_e on w.

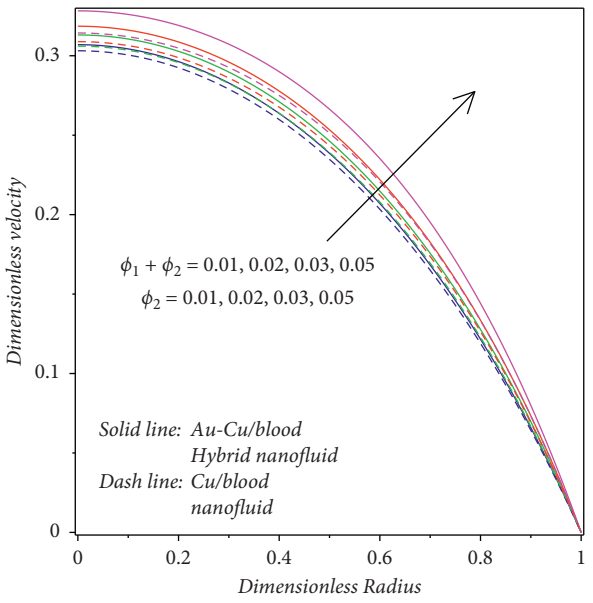

Figure 6: Behaviour of $\phi_1 + \phi_2$ and ϕ_2 on w.

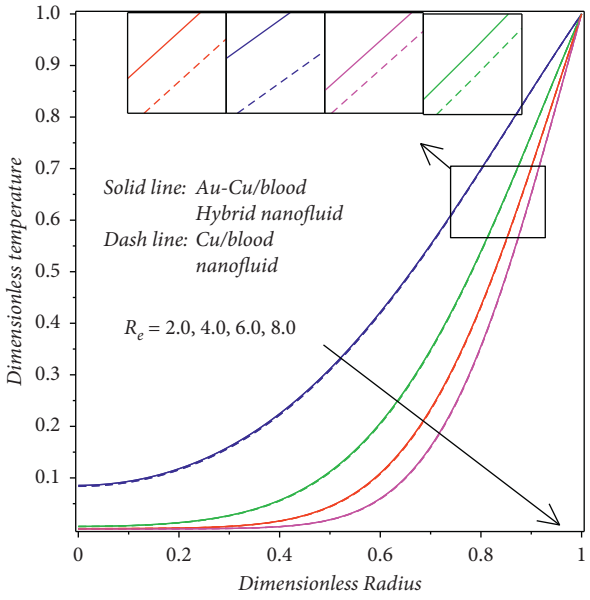

Figure 5: Behaviour of R_e on θ.

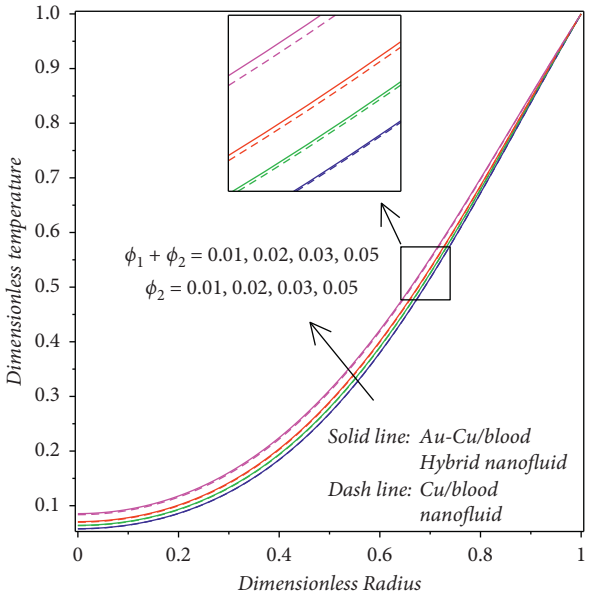

Figure 7: Behaviour of $\phi_1 + \phi_2$ and ϕ_2 on θ.

reduces while growing values of R_e. Further, blood temperature experiences a similar nature. The lower value of R_e ($R_e = 2$) exhibits less impact on the blood velocity and temperature; however, its magnitudes variation is higher by growing R_e ($R_e = 4, 6, 8$). Due to stenosis prohibition and nanoparticles, blood flow reduction occurs in the channel, even though the Reynolds number promotes the inertial force. Due to this reason, biomagnetic blood velocity and temperature are behaving with the impact of R_e.

Figures 6 and 7 demonstrate the characteristics of nanoparticles volume fraction $(\phi_1 + \phi_2)$ on blood velocity and temperature in hybrid nanofluid and nanofluid cases. It is seen from Figure 6 that the augmentation of gold-copper $(\phi_1 + \phi_2)$ nanoparticle concentration and copper (ϕ_2) nanoparticle concentration from 0.01 to 0.05 tends to promote the blood velocity in the artery. This characteristic of hybrid nanofluid is predominant to clinicians because it may help to promote the blood flow in the capillary tubes and stenosis during surgery. Figure 7 is drawn to discuss the behaviour of nanoparticles volume fraction $(\phi_1 + \phi_2)$ on blood temperature. An increment in nanoparticles

volume fraction remarkably elevates the blood temperature. Further, coupling the gold nanoparticle (ϕ_1) with copper nanoparticles (ϕ_2) highly contributes to blood temperature growth than copper nanoparticles suspension in the blood. It is revealed from this figure that the thermal diffusion of blood rises with nanoparticles in the stenotic vessel, which leads to elevating the transport process. These results show that the hybrid nanoparticles and copper nanoparticles help to accelerate the blood flow in the regular and irregular stenosis artery region.

Figure 8 is plotted to exhibit the influence of the Hartmann number (M_a) on blood velocity. In the case of $M_a = 0$, the biomagnetic blood nanofluid behave as a nonmagnetic blood nanofluid. It is found that the fluid momentum has a higher magnitude difference for M_a values 1–5. The gold and copper nanoparticles are highly dragged with the strength of Lorentz force in the artery. This creates a resistive behaviour in the blood flow. Due to this reason, blood velocity declines. Further, it is noticed that the present outcome accords with the results of Das et al. [7]. The greater diffusion of nanoparticles is the prime objective in medical applications, so that this characteristic of M_a is remarkable in synthesising bio-nanomaterials. Also, due to the characteristic of the magnetic field, it is employed to control the blood flow in the artery. It can be used to treat several cardiovascular diseases as an effective tool. In particular, this may be useful in wound treatments and pharmacological, for instance, healing skin contusions and burns.

Figure 9 explores the changes of the Grashof number (G_r) on blood hybrid nanofluid axial velocity. An increase in G_r causes to lift the blood velocity for both the hybrid and unitary nanofluid cases. It is noted that G_r is the ratio between buoyancy force and viscous force. The concentration differences of nanoparticles tend to grow the diffusion of nanoparticle species in the blood. Thus, the thermal buoyancy force increases in the channel, whereas viscous force decreases. As a result, the blood velocity rises. Figures 10 and 11 demonstrate the nature of constant heat source (β) on blood velocity and temperature. In the channel, the generation of energy takes place as a result of the increase of β. The gold and copper nanoparticles are energized with the impact of β. Besides, the heat slightly triggers the buoyancy force. Therefore, the blood nanofluid and hybrid nanofluid velocity and temperature increases. Figure 12 displays the influence of changing viscosity parameter (η_0) on blood velocity. It is observed that it has the same characteristic as G_r on fluid velocity. Physically, the viscosity of the blood lessens owing to the rising values of η_0. As a consequence, blood velocity is accelerated. Numerous values of angle parameter (α) on biomagnetic blood nanofluid velocity is displayed in Figure 13. It is evident that the blood velocity augments with the increasing values of α. In this model, α is incorporated with the thermal buoyancy term in the momentum equation. Therefore, when α is absent, it eliminates the thermal buoyancy effect in the regime. Further, rising the α highly enhances the buoyancy effect, and it accelerates the blood velocity.

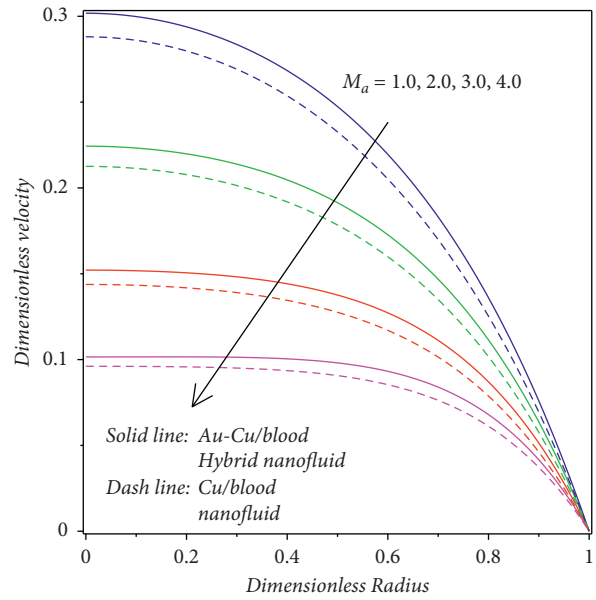

Figure 8: Behaviour of M_a on w.

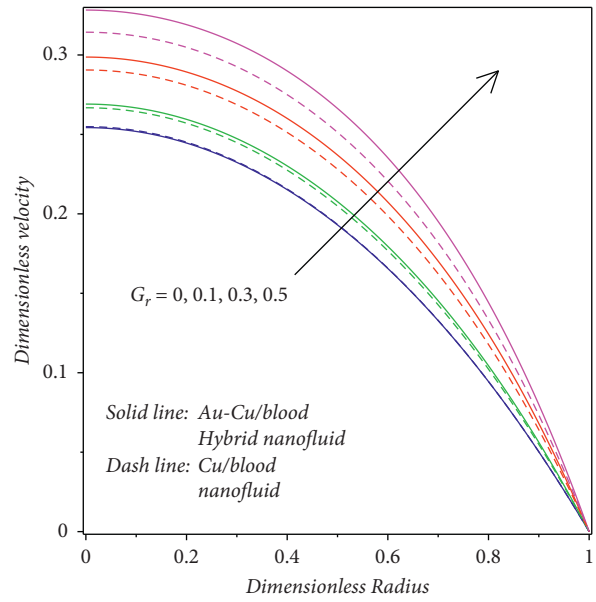

Figure 9: Behaviour of G_r on w.

Figures 14–17 depict the influences of the Grashof number (G_r), angle parameter (α), the Reynolds number (R_e), and the Hartmann number (M_a) on volumetric flow rate (Q_F) for hybrid and single nanofluid cases. It is cleared that the integration of variable blood velocity concerning the channel radial direction is known as volumetric flow rate. Besides, the volumetric flow rate reveals the nature of the axis velocity. The impacts of M_a and R_e on volumetric flow rate are illustrated in Figures 14 and 15. It is confirmed that M_a and R_e highly reduce the axial blood velocity (see

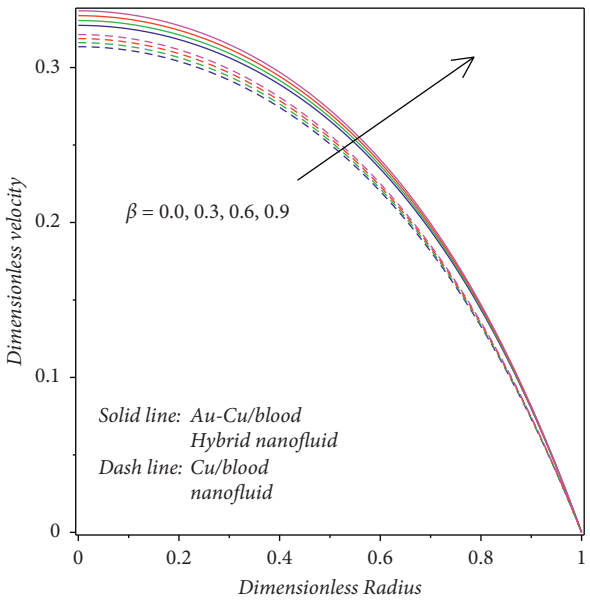

Figure 10: Behaviour of β on w.

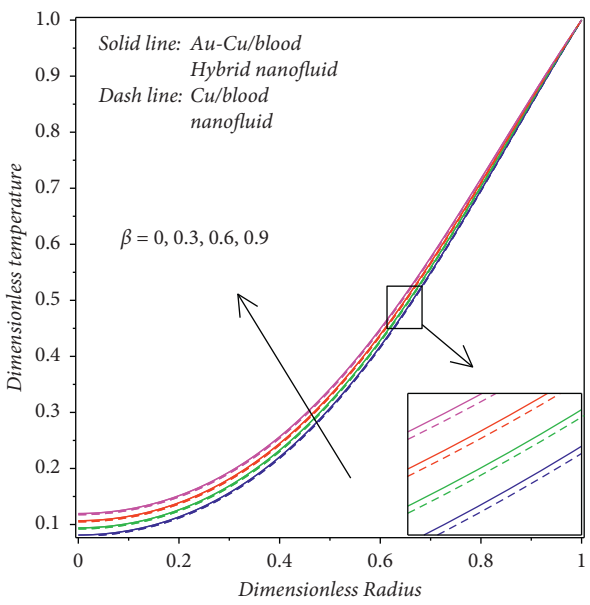

Figure 11: Behaviour of β on θ.

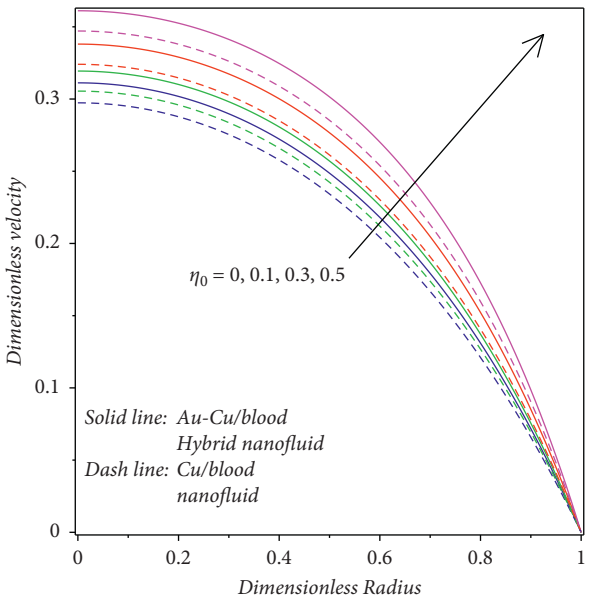

Figure 12: Behaviour of η_0 on w.

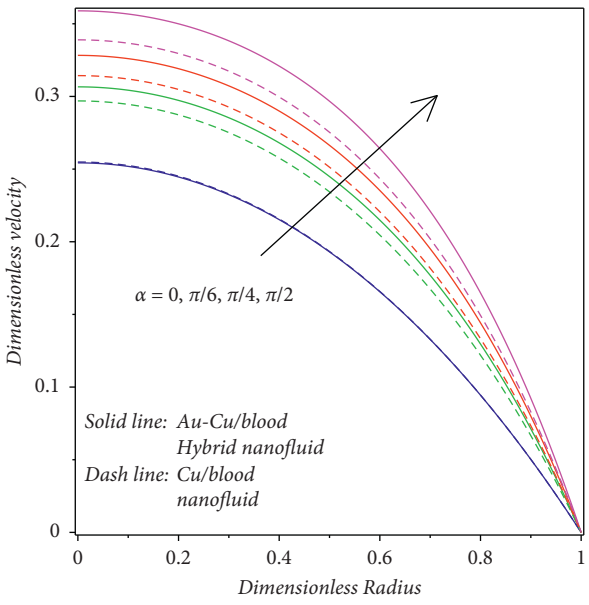

Figure 13: Behaviour of α on w.

Figures 4 and 8). M_a and R_e follow the same behaviour expressed in axial blood velocity on the volumetric flow rate. The response in volumetric flow rate to G_r and α parameters is provided in Figures 16 and 17. From these figures, it is clear that both the parameters have a similar trend. The amplification in G_r and α tends to enhance Q_F. Further, the absence of G_r and α expresses a lower Q_F; however, magnifying these parameters manifests a greater Q_F in the artery.

The behaviours of the Grashof number (G_r), angle parameter (α), changing viscosity parameter (η_0), and the Hartmann number (M_a) on the wall shear stress (τ_s) are sketched in Figures 18–21. It is evident that endothelial proliferation and turbulent flow happen in the system when low shear stress occurs. Besides, laminar flow happens with high shear stress. Figure 18 shows the impact of M_a on wall shear stress. When this term is magnified, the wall shear

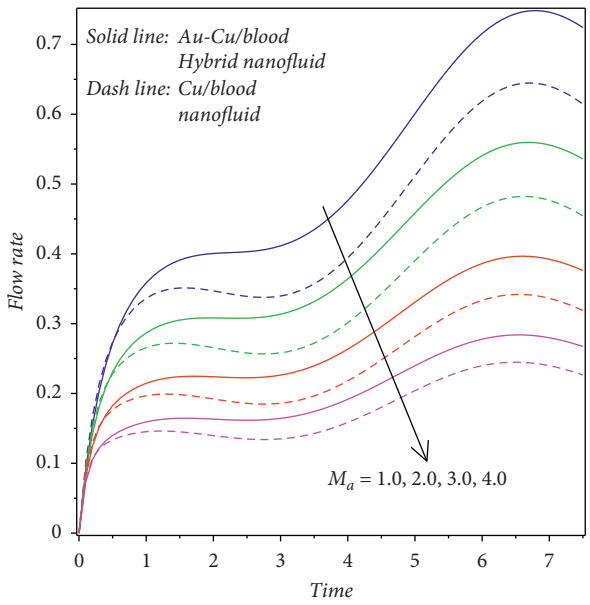

Figure 14: Behaviour of M_a on Q_F.

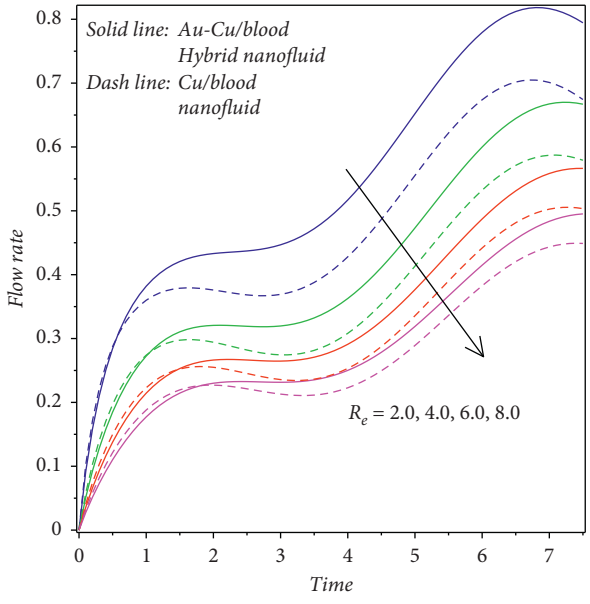

Figure 15: Behaviour of R_e on Q_F.

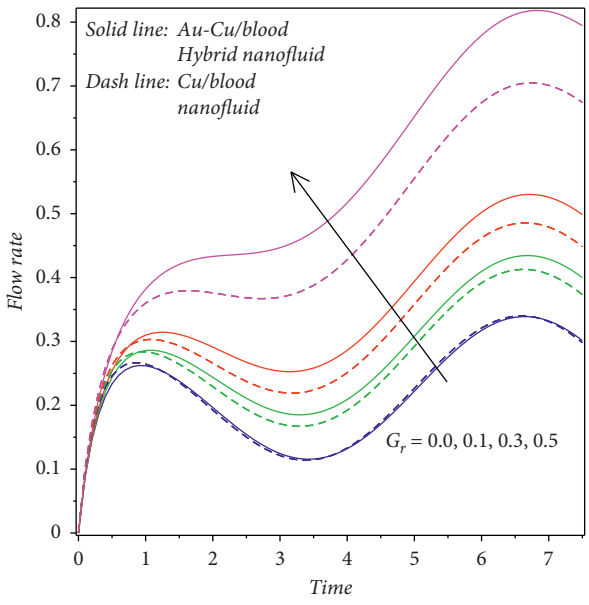

Figure 16: Behaviour of G_r on Q_F.

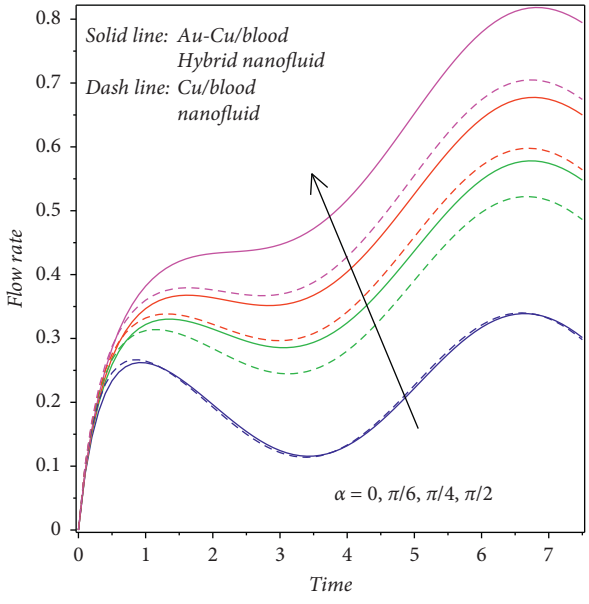

Figure 17: Behaviour of α on Q_F.

stress is reduced. It is revealed that the magnetic field plays a major role to maintain a laminar flow in the system. Figures 19–21 are drawn to explore the influences of G_r, α, and η_0 on wall shear stress. These figures show that higher values of G_r, α, and η_0 result in increasing the wall shear stress for nanofluid and hybrid nanofluid cases. It is cleared from these figures that wall shear stress (τ_s) is highly sensitive to copper (ϕ_2) nanoparticles rather than gold-copper ($\phi_1 + \phi_2$) hybrid nanoparticles.

Figures 22 and 23 present the effects of the Hartmann number (M_a) and angle parameter (α) on resistance impedance. The resistance impedance is inversely related

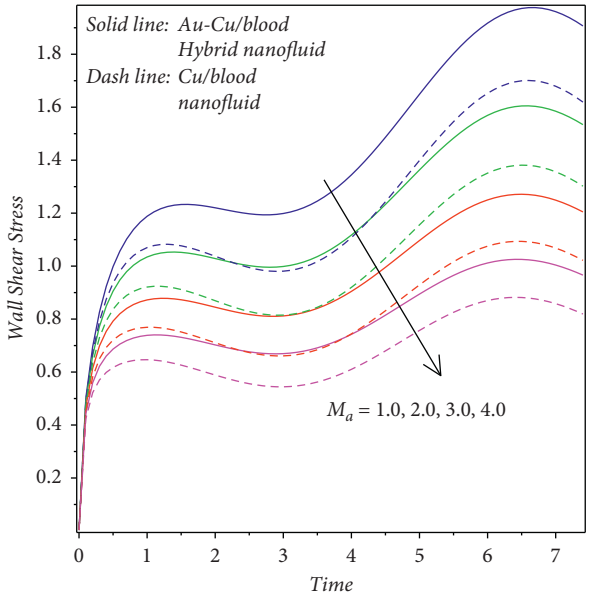

Figure 18: Behaviour of M_a on τ_s.

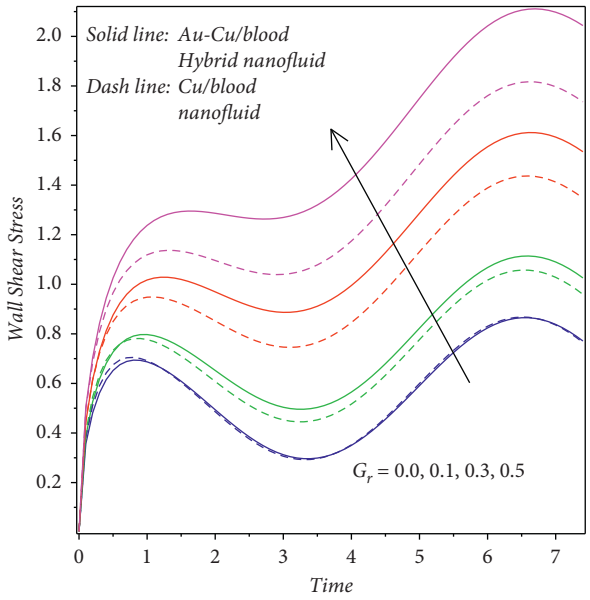

Figure 19: Behaviour of G_r on τ_s.

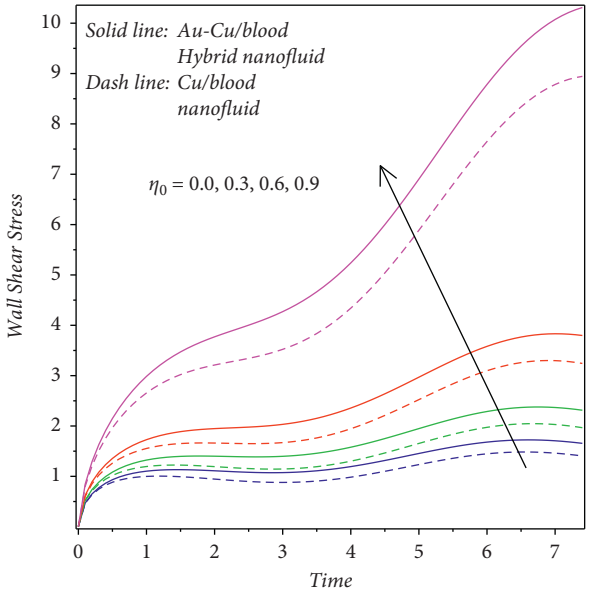

Figure 20: Behaviour of η_0 on τ_s.

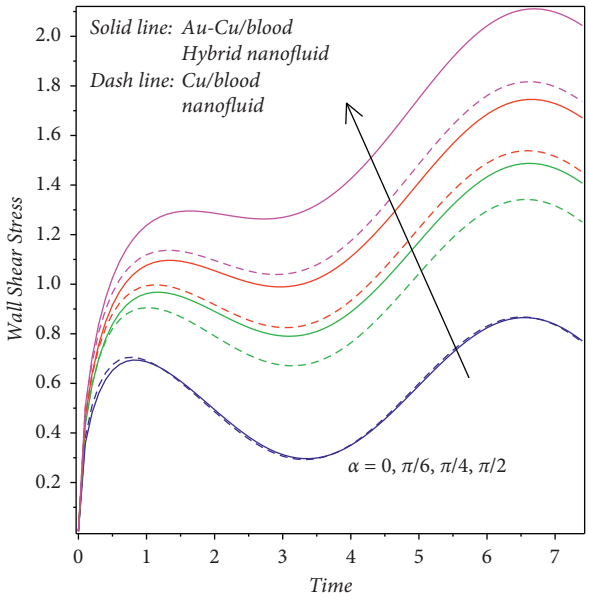

Figure 21: Behaviour of α on τ_s.

to the flow rate, which is exhibited in (18). Magnifying the magnetic field (M_a) slowdown the resistance impedance in the artery, whereas the opposite trend is found for α. This flow pattern exhibits that the growing magnetic field declines the impedance of the blood rheology. Further, the magnetic field behaves like a controlling parameter to tune the impedance effects. This result shows that controlling the blood movement in the artery thus help to stabilize the patients instantly. Figures 24 and 25 exhibit the changes in blood flow rate for several values of the

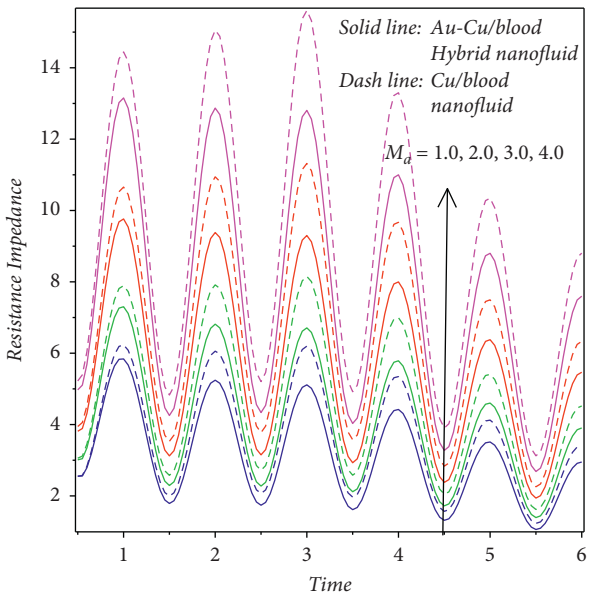

Figure 22: Behaviour of M_a on λ.

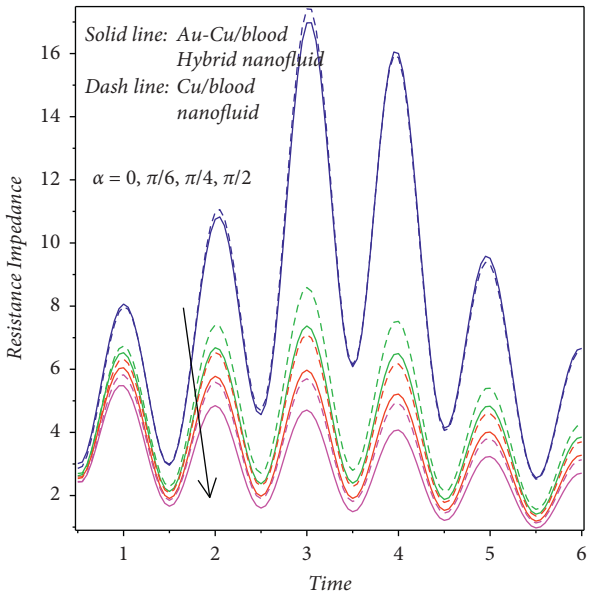

Figure 23: Behaviour of α on λ.

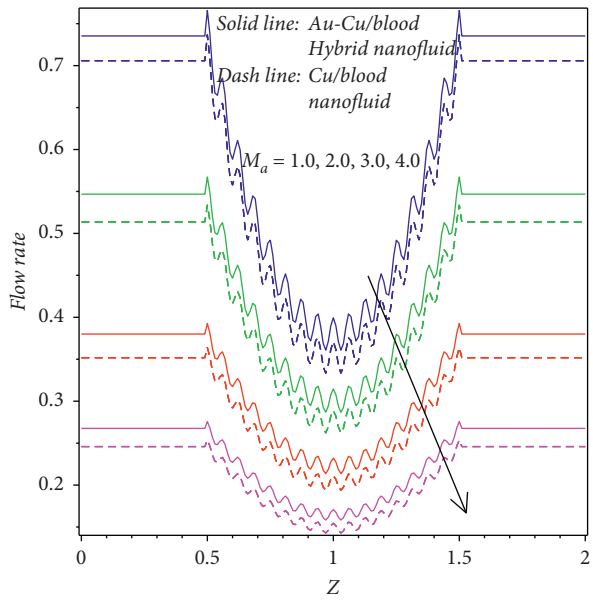

Figure 24: Behaviour of M_a on Q_F at Z.

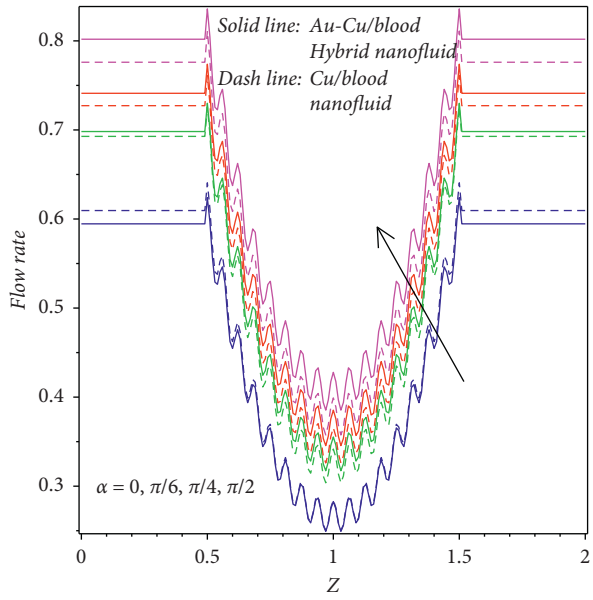

Figure 25: Behaviour of α on Q_F at Z.

Hartmann number (M_a) and angle parameter (α). It is cleared that the flow rate in the axial coordinate is elevated with the increasing values of α, whereas a reverse trend is found for M_a. The influences of ϕ_1, ϕ_2, and β on the Nusselt number (Nu^*) are depicted in Figures 26 and 27, respectively. It is ascertained that the Nusselt number is highly improved with the impacts of ϕ_1, ϕ_2, and β . Further, it is clear that the hybrid nanofluid has a supreme heat transfer rate than the copper nanofluid case.

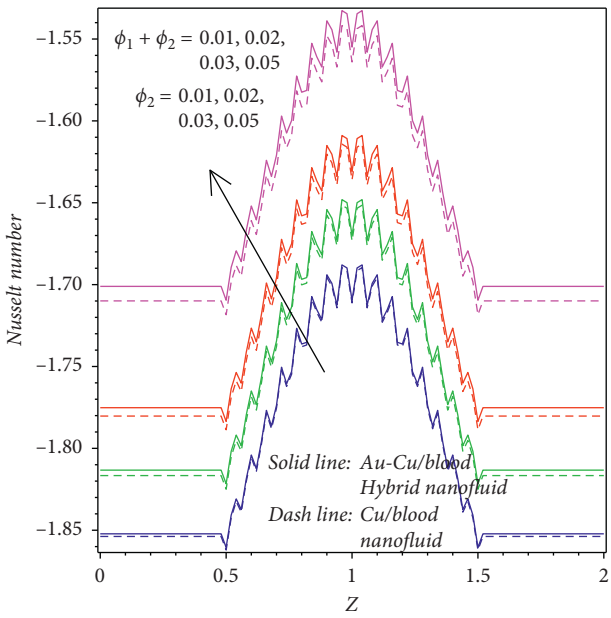

Figure 26: Behaviour of $\phi_1 + \phi_2$ and ϕ_2 on Nu* at Z .

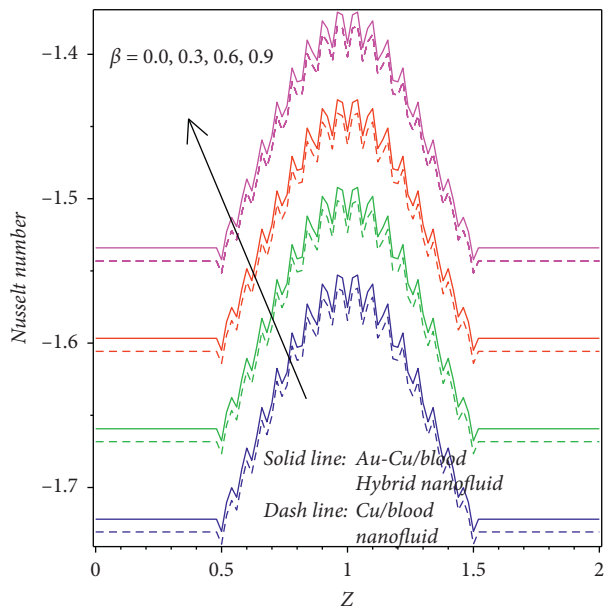

Figure 27: Behaviour of β on Nu* at Z.

5. Conclusions

The impacts of changing viscosity and Lorentz force on the biomagnetic hybrid nanofluid flow through an inclined irregular stenosis artery have been scrutinized in this study. To exhibit the characteristics of hybrid nanofluid, the volume fraction model is adopted. The mild stenosis approximation is considered to simplify governing flow equations. The nondimensionalized flow equations are solved by deploying a finite-difference approach. The present numerical solution is validated with Zaman et al. [5] and Tripathi et al. [6] for various axial velocity values, which is portrayed in Table 2. From this Table 2, it is evident that the adopted numerical method has a decent agreement. Variations caused by the influences of growing parameters on blood hybrid nanofluid velocity, temperature, and physical quantities (wall shear stress, resistance impedance, flow rate) are shown through graphs. The preeminent findings of the present analysis are itemized as follows:

(I) It is cleared that the hybrid nanoparticles have a better fluid flow and heat transfer than the unitary nanoparticles

(II) The hybrid nanoparticle and copper nanoparticle volume fraction promote the axial velocity and temperature of the blood

(III) The hybrid nanoparticles express a supreme flow rate than the copper nanoparticles

(IV) In the absence of the Grashof number and angle parameter, the wall shear stress and flow rate have similar trends for hybrid nanofluid and copper nanofluid cases

(V) The variable viscosity parameter exhibits the peak magnitude on wall shear stress by magnifying values

(VI) In the 2.5-to-3.5-time region, the Hartmann number and angle parameter manifest a greater resistance impedance on the blood hybrid nanofluid flow

(VII) Variable viscosity, heat source/sink, and angle parameter cause to enhance the blood hybrid nanofluid velocity

(VIII) The blood axial velocity in the stenosis artery decreases by means of the growing Reynolds number

Data Availability

The data used in the study are provided in the respective text part, and no additional data are employed for these outcomes.

Conflicts of Interest

The authors declare that they have no conflicts of interest.

Acknowledgments

This work was funded by the Chennai Institute of Technology, India, vide funding number CIT/CNS/2021/RD/064.

References

[1] M. N. Krishnan, "Coronary heart disease and risk factors in India - on the brink of an epidemic?" *Indian Heart Journal*, vol. 64, no. 4, pp. 364–367, 2012.

[2] R. Gupta, I. Mohan, and J. Narula, "Trends in coronary heart disease epidemiology in India," *Annals of Global Health*, vol. 82, no. 2, pp. 307–15, 2016.

[3] J. V. Ramana Reddy, D. Srikanth, and S. K. Das, "Modelling and simulation of temperature and concentration dispersion

in a couple stress nanofluid flow through stenotic tapered arteries," *The European Physical Journal Plus*, vol. 132, no. 8, p. 365, 2017.

[4] S. Changdar and S. De, "Investigation of nanoparticle as a drug carrier suspended in a blood flowing through an inclined multiple stenosed artery," *BioNanoScience*, vol. 8, no. 1, pp. 166–178, 2018.

[5] A. Zaman, N. Ali, and A. A. Khan, "Computational biomedical simulations of hybrid nanoparticles on unsteady blood hemodynamics in a stenotic artery," *Mathematics and Computers in Simulation*, vol. 169, pp. 117–132, 2020.

[6] J. Tripathi, B. Vasu, and O. A. Bég, "Computational simulations of hybrid mediated nano- hemodynamics (Ag-Au/Blood) through an irregular symmetric stenosis," *Computers in Biology and Medicine*, vol. 130, Article ID 104213, 2021.

[7] S. Das, T. K. Pal, R. N. Jana, and B. Giri, "Significance of Hall currents on hybrid nano-blood flow through an inclined artery having mild stenosis: homotopy perturbation approach," *Microvascular Research*, vol. 137, Article ID 104192, 2021.

[8] J. Prakash and O. D. Makinde, "Radiative heat transfer to blood flow through a stenotic artery in the presence of magnetic field," *Latin American Applied Research*, vol. 41, no. 3, pp. 273–277, 2011.

[9] M. M. Rashidi, M. Keimanesh, O. A. Bég, and T. K. Hung, "Magnetohydrodynamic biorheological transport phenomena in a porous medium: a simulation of magnetic blood flow control and filtration," *International Journal for Numerical Methods in Biomedical Engineering*, vol. 27, no. 6, pp. 805–821, 2011.

[10] M. Rashidi, M. Bhatti, M. Abbas, and M. Ali, "Entropy generation on MHD blood flow of nanofluid due to peristaltic waves," *Entropy*, vol. 18, no. 4, p. 117, 2016.

[11] R. Ponalagusamy and S. Priyadharshini, "Numerical modelling on pulsatile flow of Casson nanofluid through an inclined artery with stenosis and tapering under the influence of magnetic field and periodic body acceleration," *Korea-Australia Rheology Journal*, vol. 29, no. 4, pp. 303–316, 2017.

[12] S. Noreen, M. M. Rashidi, and M. Qasim, "Blood flow analysis with considering nanofluid effects in vertical channel," *Applied Nanoscience*, vol. 7, no. 5, pp. 193–199, 2017.

[13] H. T. Basha and R. Sivaraj, "Numerical simulation of blood nanofluid flow over three different geometries by means of gyrotactic microorganisms: applications to the flow in a circulatory system," *Proceedings of the Institution of Mechanical Engineers - Part C: Journal of Mechanical Engineering Science*, vol. 235, no. 2, pp. 441–460, 2020.

[14] M. U. Ashraf, M. Qasim, A. Wakif, M. I. Afridi, and I. L. Animasaun, "A generalized differential quadrature algorithm for simulating magnetohydrodynamic peristaltic flow of blood-based nanofluid containing magnetite nanoparticles: a physiological application," *Numerical Methods for Partial Differential Equations*, pp. 1–27, 2020.

[15] H. T. Basha and R. Sivaraj, "Exploring the heat transfer and entropy generation of Ag/Fe$$_3$$O$$_4$$-blood nanofluid flow in a porous tube: a collocation solution," *The European Physical Journal E*, vol. 44, no. 3, p. 31, 2021.

[16] S. Rathore and D. Srikanth, "Mathematical study of transport phenomena of blood nanofluid in a diseased artery subject to catheterization," *Indian Journal of Physics*, vol. 106, 2021.

[17] H. Basha and R. Sivaraj, "Entropy generation of peristaltic Eyring-Powell nanofluid flow in a vertical divergent channel for biomedical applications," *Proceedings of the Institution of Mechanical Engineers - Part E: Journal of Process Mechanical Engineering*, vol. 235, no. 5, pp. 1575–1586, 2021.

[18] J. C. Misra, "Biomagnetic viscoelastic fluid flow over a stretching sheet," *Applied Mathematics and Computation*, vol. 210, no. 2, pp. 350–361, 2009.

[19] M. G. Murtaza, M. Ferdows, J. C. Misra, and E. E. Tzirtzilakis, "Three-dimensional biomagnetic Maxwell fluid flow over a stretching surface in presence of heat source/sink," *International Journal of Biomathematics*, vol. 12, no. 3, Article ID 1950036, 2019.

[20] S. Maiti and S. Shaw, "Caputo-Fabrizio fractional order model on MHD blood flow with heat and mass transfer through a porous vessel in the presence of thermal radiation," *Physica A: Statistical Mechanics and Its Applications*, vol. 540, Article ID 123149, 2019.

[21] S. M. Mousavi, A. A. R. Darzi, O. a. Akbari, D. Toghraie, and A. Marzban, "Numerical study of biomagnetic fluid flow in a duct with a constriction affected by a magnetic field," *Journal of Magnetism and Magnetic Materials*, vol. 473, pp. 42–50, 2019.

[22] S. R. El Koumy, E. S. I. Barakat, and S. I. Abdelsalam, "Hall and porous boundaries effects on peristaltic transport through porous medium of a maxwell model," *Transport in Porous Media*, vol. 94, no. 3, pp. 643–658, 2012.

[23] S. Changdar and S. De, "Analytical investigation of nanoparticle as a drug carrier suspended in a MHD blood flowing through an irregular shape stenosed artery," *Iranian Journal of Science and Technology*, vol. 43, no. 1, pp. 1259–1272, 2017.

[24] Y. A. Elmaboud and S. I. Abdelsalam, "DC/AC magneto-hydrodynamic-micropump of a generalized Burger's fluid in an annulus," *Physica Scripta*, vol. 94, no. 11, Article ID 115209, 2019.

[25] M. M. Bhatti, S. Z. Alamri, R. Ellahi, and S. I. Abdelsalam, "Intra-uterine particle-fluid motion through a compliant asymmetric tapered channel with heat transfer," *Journal of Thermal Analysis and Calorimetry*, vol. 144, no. 6, pp. 2259–2267, 2020.

[26] S. I. Abdelsalam, J. X. Velasco-Hernández, and A. Z. Zaher, "Electro-magnetically modulated self-propulsion of swimming sperms via cervical canal," *Biomechanics and Modeling in Mechanobiology*, vol. 20, pp. 861–878, 2020.

[27] A. Chatterjee, S. Changdar, and S. De, "Study of nanoparticle as a drug carrier through stenosed arteries using Bernstein polynomials," *International Journal for Computational Methods in Engineering Science and Mechanics*, vol. 21, no. 5, pp. 243–251, 2020.

[28] B. Bhaumik, S. Changdar, and S. De, "Combined impact of Brownian motion and thermophoresis on nanoparticle distribution in peristaltic nanofluid flow in an asymmetric channel," *International Journal of Ambient Energy*, pp. 1–12, 2021.

[29] K. S. Mekheimer, R. E. Abo-Elkhair, S. I. Abdelsalam, K. K. Ali, and A. M. A. Moawad, "Biomedical simulations of nanoparticles drug delivery to blood hemodynamics in diseased organs: synovitis problem," *International Communications in Heat and Mass Transfer*, vol. 130, p. 105756, 2022.

[30] M. A. Abbas, Y. Q. Bai, M. M. Rashidi, and M. M. Bhatti, "Application of drug delivery in magnetohydrodynamics peristaltic blood flow of nanofluid in a non-uniform channel," *Journal of Mechanics in Medicine and Biology*, vol. 16, no. 4, Article ID 1650052, 2016.

[31] H. Thameem Basha, R. Sivaraj, A. Subramanyam Reddy, and A. J Chamkha, "SWCNH/diamond-ethylene glycol nanofluid flow over a wedge, plate and stagnation point with induced

magnetic field and nonlinear radiation - solar energy application," *The European Physical Journal - Special Topics*, vol. 228, no. 12, pp. 2531–2551, 2019.

[32] H. Shojaie Chahregh and S. Dinarvand, "TiO2-Ag/blood hybrid nanofluid flow through an artery with applications of drug delivery and blood circulation in the respiratory system," *International Journal of Numerical Methods for Heat and Fluid Flow*, vol. 30, no. 11, pp. 4775–4796, 2020.

[33] P. B. A. Reddy, "Biomedical aspects of entropy generation on electromagnetohydrodynamic blood flow of hybrid nanofluid with nonlinear thermal radiation and non-uniform heat source/sink," *The European Physical Journal Plus*, vol. 135, no. 10, p. 852, 2020.

[34] E. H. Jeong, G. Jung, C. A. Hong, and H. Lee, "Gold nanoparticle (AuNP)-based drug delivery and molecular imaging for biomedical applications," *Archives of Pharmacal Research*, vol. 37, no. 1, pp. 53–59, 2014.

[35] M. Sengani, A. M. Grumezescu, and V. D. Rajeswari, "Recent trends and methodologies in gold nanoparticle synthesis - a prospective review on drug delivery aspect," *Open*, vol. 2, pp. 37–46, 2017.

[36] N. S. Aminabad, M. Farshbaf, and A. Akbarzadeh, "Recent advances of gold nanoparticles in biomedical applications: state of the art," *Cell Biochemistry and Biophysics*, vol. 77, no. 2, pp. 123–137, 2019.

[37] M. Vairavel, E. Devaraj, and R. Shanmugam, "An eco-friendly synthesis of Enterococcus sp.-mediated gold nanoparticle induces cytotoxicity in human colorectal cancer cells," *Environmental Science and Pollution Research*, vol. 27, no. 8, pp. 8166–8175, 2020.

[38] X. Chen, X. Zhao, and G. Wang, "Review on marine carbohydrate-based gold nanoparticles represented by alginate and chitosan for biomedical application," *Carbohydrate Polymers*, vol. 244, Article ID 116311, 2020.

[39] O. K. Koriko, I. L. Animasaun, B. Mahanthesh, S. Saleem, G. Sarojamma, and R. Sivaraj, "Heat transfer in the flow of blood-gold Carreau nanofluid induced by partial slip and buoyancy," *Heat Transfer - Asian Research*, vol. 9, no. 6, pp. 1–18, 2018.

[40] P. Bharath Kumar and S. Srinivas, "Pulsating flow of a non-Newtonian nanofluid in a porous channel with magnetic field," *Materials Today Proceedings*, vol. 9, no. 2, pp. 320–332, 2019.

[41] U. Khan, S. Bilal, A. Zaib, O. D. Makinde, and A. Wakif, "Numerical simulation of a nonlinear coupled differential system describing a convective flow of Casson gold–blood nanofluid through a stretched rotating rigid disk in the presence of Lorentz forces and nonlinear thermal radiation," *Numerical Methods for Partial Differential Equations*, pp. 1–21, 2020.

[42] M. M. Bhatti, "Biologically inspired intra-uterine nanofluid flow under the suspension of magnetized gold (Au) nanoparticles: applications in nanomedicine," *Inventions*, vol. 6, no. 2, p. 28, 2021.

[43] K. A. Hoffman and S. T. Chiang, "Computational fluid dynamics. Engineering education system," *Kansas*, vol. 1, p. 486, 2000.

[44] O. A. Bég, M. S. Khan, I. Karim, M. M. Alam, and M. Ferdows, "Explicit numerical study of unsteady hydromagnetic mixed convective nanofluid flow from an exponentially stretching sheet in porous media," *Applied Nanoscience*, vol. 4, no. 8, pp. 943–957, 2014.

[45] J. Tripathi, B. Vasu, O. A. Bég, R. S. R. Gorla, and P. K. Kameswaran, "Computational simulation of rheological blood flow containing hybrid nanoparticles in an inclined catheterized artery with stenotic, aneurysmal and slip effects," *Computers in Biology and Medicine*, vol. 139, Article ID 105009, 2021.

[46] A. Zaman, N. Ali, and N. Kousar, "Nanoparticles (Cu, TiO2, Al2O3) analysis on unsteady blood flow through an artery with a combination of stenosis and aneurysm," *Computers & Mathematics with Applications*, vol. 76, no. 9, pp. 2179–2191, 2018.

[47] K. S. Mekheimer, B. M. Shankar, S. F. Ramadan, H. E. Mallik, and M. S. Mohamed, "On the stability of convection in a non-Newtonian vertical fluid layer in the presence of gold nanoparticles: drug agent for thermotherapy," *Mathematics*, vol. 9, no. 11, p. 1302, 2021.

[48] A. C. Burton, "Physiology and biophysics of the circulation," *Introductory Text*, Year Book Medical Publisher, Chicago, 1966.

[49] O. A. Bég, N. Ali, A. Zaman, E. T. A. Bég, and A. Sohail, "Computational modeling of heat transfer in an annular porous medium solar energy absorber with the P1-radiative differential approximation," *Journal of the Taiwan Institute of Chemical Engineers*, vol. 66, pp. 258–268, 2016.

[50] A. Zaman, N. Ali, O. Anwar Bég, and M. Sajid, "Heat and mass transfer to blood flowing through a tapered overlapping stenosed artery," *International Journal of Heat and Mass Transfer*, vol. 95, pp. 1084–1095, 2016.

[51] F. Sultan, N. A. Khan, and M. I. Afridi, "Investigation of biological mechanisms during flow of nano-Bingham-Papanastasiou fluid through a diseased curved artery," *Part N: Journal of Nanomaterials, Nanoengineering and Nanosystems*, vol. 234, no. 3, pp. 69–81, 2020.